THE JOURNAL OF PHYSICAL CHEMISTRY C

Article

Cite This: J. Phys. Chem. C XXXX, XXX, XXX−XXX

pubs.acs.org/JPCC

Modeling the Formation and Propagation of VO_x Islands on Rh(111) under Reactive Conditions

Yannick De Decker,*[,†] Amir Raghamy,[†] and Ronald Imbihl[‡]

[†]Center for Nonlinear Phenomena and Complex Systems (CENOLI) and Nonlinear Physical Chemistry Unit, Université libre de Bruxelles (ULB), Campus Plaine, C.P. 231, B-1050 Brussels, Belgium

[‡]Institut für Physikalische Chemie und Elektrochemie, Leibniz-Universität Hannover, Callinstrasse 3A, D-30167 Hannover, Germany

ABSTRACT: Phase transitions between different states of a system often involve a long-term maturation process known as ripening, whose mechanism can take various forms. Recent experimental investigations on phase transitions involving vanadium oxides on rhodium have shown the existence of a new ripening mechanism, during which micrometric islands of a dense VO_x phase move and coalesce exclusively in the presence of a catalytic reaction. It was hypothesized that this new pathway is fueled by an underlying polymerization/depolymerization process. In this work, we develop a generic reaction-diffusion model containing the basic physicochemical ingredients of these systems. This model reproduces qualitatively the observed behaviors and confirms that it can be traced back to an interplay between intermolecular interactions and the nonequilibrium polymerization process.

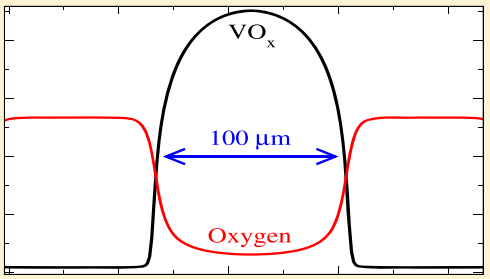

INTRODUCTION

Investigations of catalytic metal surfaces have revealed the existence of numerous complex spatiotemporal dynamics.[1−3] The appearance of these dynamical behaviors can be traced back to a combination of several factors. First, surface reactions are usually studied far from thermodynamic equilibrium so that dissipative structures[4] can, at least in principle, emerge. Second, surface reactions typically include nonlinear processes associated with feedback loops. Another important feature of these systems is the presence of repulsive or attractive energetic interactions between adsorbates. These "lateral" interactions can induce the formation of ordered overlayers. The combination of nonlinearity, nonequilibrium conditions, and lateral interactions leads to the emergence of complex structures.

In the present paper, we will be interested in recent observations made during the catalytic oxidation of various simple molecules on vanadium oxide (VO_x)-covered rhodium surfaces. At equilibrium, VO_x species are known to form various types of ordered structures on Rh(111) depending on temperature, oxygen content, etc.[5−9] These structures take the form of well-defined VO_x islands in which vanadium and oxygen adatoms assume ordered nanostructures. Under nonequilibrium conditions, i.e., if a catalytic reaction takes place on such VO_x-covered surfaces, new mesoscopic structures can emerge.[10−15] Striped patterns with a characteristic size ranging between 10 and 100 μm were for example observed on Rh(111)/VO_x during exposure to H_2 + O_2 gas mixtures.[10−12] Micrometric stripes and round islands were also reported during oxidation of methanol, CO, and ammonia in the same system.[13,14] The round islands were shown to correspond to dense VO_x domains. Remarkably, it was reported that these VO_x-rich islands can move and merge exclusively under reactive conditions, a phenomenon that constitutes a new chemistry-based mechanism for island ripening.[13]

Our objective here will be to rationalize these observations by modeling the system under consideration as a nonequilibrium surface reaction in the presence of lateral interactions. We will not focus on one of the aforementioned reactions in particular but will instead devise a generic model containing all of the basic features that these systems share. To this end, we first summarize the main experimental findings (Experiments). Theory is devoted to the derivation of a generic reaction-diffusion model for the class of systems under consideration. Phase Transitions in Homogeneous Systems focuses on the derivation of general conditions for having reactive phase separation in the derived model, while Spatiotemporal Simulations presents numerical results of pattern formation and island movement and merging. We discuss in particular how one can derive a law of motion for the islands, based on a balance of effective forces acting on them. Finally, in the Conclusions, we summarize our findings and discuss possible implications and extensions of this work.

EXPERIMENTS

It is well established that two-dimensional VO_x structures of various stoichiometries can be found on Rh(111).[5−9] One

Received: January 15, 2019
Revised: April 3, 2019
Published: April 12, 2019

DOI: 10.1021/acs.jpcc.9b00427
J. Phys. Chem. C XXXX, XXX, XXX−XXX

typically observes well-defined islands consisting of ordered phases whose unit cell is on the order of an Angström. Interestingly, most of these structures can be seen as networks of VO_5 pyramids sharing oxygen corner atoms. The different reported stoichiometries correspond to varying types of connections between these pyramids.

Imbihl et al. have studied the properties of this system during catalytic reactions.[10−15] In these experiments, VO_x deposition was first conducted by reactive evaporation on Rh(111), during which vanadium was evaporated in the presence of oxygen. The surface coverage of vanadium was usually lower than or equal to 0.5 MLE (monolayer equivalent or number of V atoms per substrate atom). Because of the small characteristic length of the structures found in the absence of catalytic reactions, the surface appears at this stage homogeneous upon observation with a photoemission electron microscope (PEEM). This homogeneous state can be lifted by exposing the sample to gaseous reactants participating in a oxidation process on the surface. For temperatures between 550 and 650 °C, stripes with a characteristic size ranging from a few to a few hundred micrometers emerge. At higher temperature, the stripes first coarsen and then merge to form almost circular spots of various sizes. An example of such structures is given in Figure 1, in the case of the $CH_3OH + O_2$

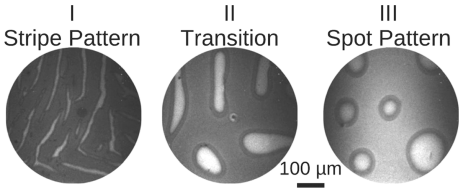

Figure 1. Patterns observed in the VO_x/Rh(111) system at temperatures T = 550 °C (I), 650 °C (II), and 700 °C (III). Experimental conditions: vanadium coverage = 0.23 MLE, partial pressure of methanol = partial pressure of dioxygen = 1×10^{-4} mbar.[13]

reaction. Similar organizations were also observed for the $H_2 + O_2$,[10−12] $NH_3 + O_2$, and $CO + O_2$[14] reactions and are thus quite generic. Further experiments demonstrated that the stripes and spots consist of dense VO_x phases, while the rest of the surface is covered with only a small amount of vanadium. In what follows, we will thus refer to the VO_x-rich regions as "VO_x islands".

These islands are often seen to move and merge.[14] More precisely, islands that are initially separated by a distance smaller than a critical value of ≈100 μm start to move, then deform into an oval shape, and continue their displacement toward each other until they merge (see Figure 2 for an example).

After merging, the islands slowly reorganize and recover a circular shape for long enough times. Remarkably, the island movement can be immediately stopped by removing one of the two reactants from the gas phase. These observations have led to the idea that movement and merging are here chemically induced.[13] The main hypothesis is that the islands are constantly forming and decomposing due to polymerization (depolymerization) of the VO_x dense phase from (into) "monomers". The stoichiometry of this process is such that polymerization is expected to be favored under oxygen-poor conditions. Now because of the oxidation reaction taking place in the islands, there is a gradient of oxygen around each of

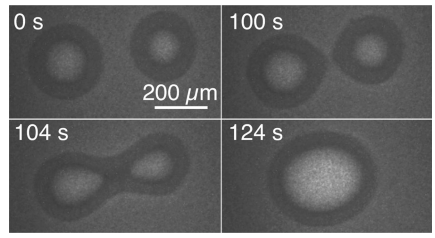

Figure 2. PEEM images of the coalescence of VO_x islands under reaction conditions. Experimental conditions are the same as in Figure 1, except for T = 750 °C.[13]

them. If two islands are sufficiently close, these gradients overlap and create a region of depletion in adsorbed O. The presence of this oxygen-poor region induces a directed polymerization of the dense phase in the gap separating the islands. The islands would thus grow in this direction and at the same time dissolve in the more oxygen-rich regions, leading to their effective displacement as a whole. In the next section, we formalize these ideas by casting them in the form of a reaction-diffusion system.

THEORY

Numerous processes are expected to take place on the Rh(111) surface during the aforementioned experiments. Our objective here is to build a simple, yet representative, reaction-diffusion model for this system by including the processes that are thought to be central to the observed dynamics.

Chemical Species and Reactions. Vanadium oxides can be found on Rh(111) either as single monomers or in the form of ultrathin clusters ("polymers"). Diffusing V_6O_{12} starlike monomers have been observed at 300 K with scanning tunneling microscopy,[16] but the structure of the monomers cannot be determined at the high temperatures used in the experiments we are modeling. The fact that most of the VO_x polymerized structures and stoichiometries at high temperature can be seen as collections of VO_5 pyramids sharing corners suggests that the monomers can simply be represented by VO_5 structures.

In the absence of definitive conclusion concerning the nature of the monomers and in order to remain as general as possible, we will consider that an adsorbed VO_x species can exist either as a generic monomer M or as a polymerized unit P and that these species are involved in a polymerization/depolymerization process of the type

$$\mathrm{P} + \mathrm{M} + [*, \mathrm{O}] \underset{k_\mathrm{D}}{\overset{k_\mathrm{P}}{\rightleftharpoons}} 2\mathrm{P} + \mathrm{O} \tag{1}$$

where O represents an adsorbed oxygen atom and the [*,O] symbol stands for an unoccupied adsorption site for O, while k_P and k_D are the reaction rate constants for polymerization and depolymerization, respectively. This process is representative of the fact that polymerized units share oxygen atoms and that, consequently, monomers must release at least one oxygen atom when attaching to a polymer. The released oxygen adatom occupies an empty surface site, which is thus required for attachment to proceed. Using the law of mass action, the rate of this reaction reads

$$R_\mathrm{PD} = k_\mathrm{P} a_\mathrm{P} a_\mathrm{M} a_{*,\mathrm{O}} - k_\mathrm{D} a_\mathrm{P}^2 a_\mathrm{O} \tag{2}$$

DOI: 10.1021/acs.jpcc.9b00427
J. Phys. Chem. C XXXX, XXX, XXX−XXX

where a_i are the activities of the species involved (see Lateral Interactions for more details on how to evaluate these activities).

A crucial aspect in the observed behaviors is that the oxygen released in this way also enters a catalytic reaction. In the experiments, this reaction is the oxidation of methanol or other molecules under constant partial pressures of the two reactants in the gas phase. Thus, in addition to the polymerization/depolymerization process (eq 1), oxygen is also involved in an adsorption/desorption process and in a surface reaction. The adsorption of O_2(g) on Rh(111) is supposed to be dissociative in view of the high temperature at which experiments are performed

$$O_2(g) + 2[*, O] \underset{k_d}{\overset{k_a}{\rightleftharpoons}} 2O \tag{3}$$

In the above equation, k_a and k_d stand for the kinetic constants associated with adsorption and desorption, respectively. Assuming a Langmuir-type mechanism of adsorption, the total rate of the adsorption/desorption process is given by

$$R_{ads} = k_a p_{O_2} a_{*,O}^2 - k_d a_O^2 \tag{4}$$

Oxygen adatoms can also oxidize a reactant X, leading to products that we expect to rapidly leave the surface

$$O + X \xrightarrow{k_r} [*, O] + XO(g) \tag{5}$$

where we introduced the rate constant k_r. The species X may represent an adsorbed hydrogen adatom, in the case of the H_2 + O_2 reaction, or a CH_3O or CH_2O intermediate for the reaction with methanol.[17] We consider here X to be adsorbed on a specific set of active sites, which are different from those occupied by M, P, or O. The rate of reaction reads

$$R_{reac} = k_r a_O a_X \tag{6}$$

For simplicity, we will consider, in what follows, that the concentration in X is constant so that its activity can be incorporated in the rate constant k_r. Note that at the temperatures of interest, we expect k_d to be much smaller than k_r, so that the rate of consumption of O due to desorption should be much less than the rate of reaction. Steps (1), (3), and (5) and the corresponding rates form the core of our model.

Lateral Interactions. Adsorbed molecules and atoms exert energetic interactions on each other.[18] In our case, this is reflected by the experimental observation that VO_x islands present round shapes, have strong internal cohesion and are, so to say, immobile in the absence of nonequilibrium reactions. These properties suggest that the interactions between P species must be substantial, leading the polymerized phase to behave like a two-dimensional dense phase. On the other hand, the monomers M and the oxygen adatoms O are in a rather dilute phase and interactions are probably much weaker for these species. We will consequently consider that the dominant lateral interactions in the system are the interactions between two P species. To quantify this interaction, we introduce a potential

$$U(\mathbf{r}) = \int u(\mathbf{r}' - \mathbf{r})\theta_P(\mathbf{r}')\, d\mathbf{r}' \tag{7}$$

In the above equation, $\mathbf{r}$ is the position in space, u represents the pairwise interaction potential between two polymerized units, and θ_P is the local coverage in P (the fraction of surface sites occupied by P). The intensity of the attractive interactions between P species is expected to decrease with distance. Different choices for $u(\mathbf{r})$ respecting this condition are possible. We will use for simplicity a Gaussian shape

$$u(\mathbf{r}' - \mathbf{r}) = \frac{u_0}{(2\pi)^{d/2}\sigma} \exp\left[-\frac{(\mathbf{r}' - \mathbf{r})^2}{2\sigma^2}\right] \tag{8}$$

in which d is the dimensionality of the system, u_0 is the maximal intensity of the potential, and σ represents a characteristic interaction length. Similar potentials have been used to successfully model similar surface reactions.[19−24]

The presence of lateral interactions has consequences on the rates of the processes introduced in the previous subsection. Indeed, standard thermodynamic relations[25] show that the chemical potential of an adsorbed species i reads

$$\mu_i(\mathbf{r}) = \mu_i^0 + k_B T \ln a_i(\mathbf{r}) = \mu_i^0 + k_B T \ln \theta_i(\mathbf{r}) + U_i(\mathbf{r}) \tag{9}$$

where θ_i is the coverage of species i and U_i is the potential energy due to interactions. This has the consequence that in the evolution laws (2), (4), and (6) the activities (and thus the rates) are local quantities given by

$$a_M(\mathbf{r}) = \theta_M(\mathbf{r});\ a_O(\mathbf{r}) = \theta_O(\mathbf{r});\ a_{*,O}(\mathbf{r}) = \theta_{*,O}(\mathbf{r});\ a_P(\mathbf{r}) = \theta_P(\mathbf{r}) \exp\left[\frac{U(\mathbf{r})}{k_B T}\right]$$

As we will see in the next subsection, this will also influence the equations for the transport of adsorbates.

In addition to these lateral interactions, we need to account for the fact that the reaction between O and X does not proceed as efficiently on the bare Rh(111) surface as it does on the VO_x islands, which are the actual catalysts of the reaction for the experimental conditions we focus on. For example, at the temperature where island formation and movement are observed (700−750 °C), the reaction between methanol and oxygen almost exclusively takes place on the islands, where the rate of reaction is at least one order of magnitude faster than on the bare surface. To incorporate this in the model, we consider that the reaction rate constant k_r depends on the local coverage in polymerized units

$$k_r(\mathbf{r}) = k_r^0 \exp[\gamma\theta_P(\mathbf{r})] \tag{10}$$

in which γ is a positive constant controlling the catalytic efficiency of the VO_x polymer.

Transport. Transport is at the heart of the reported island ripening process. We here detail how we include it in the simple model. M and P species can a priori both move, although it is obvious from experimental observations that molecular movement in the large islands is rather limited. In any case, we will include the possibility to have both species moving. Neglecting cross-diffusion, the diffusive flux of a species i is proportional to the diffusive driving force in the linear regime of nonequilibrium thermodynamics[26,27]

$$\mathbf{J}_i = -L_{ii}\nabla\frac{\mu_i - \mu_S}{T} \tag{11}$$

In this equation, L_{ii} is the Onsager coefficient and μ_S is the chemical potential of the "solvent", i.e., of the species with respect to which diffusion is defined. For surface processes, this reference species is naturally set to be the fraction of active sites available to species i, $\theta_{*,i}$. Imposing that Fick's law should

DOI: 10.1021/acs.jpcc.9b00427
J. Phys. Chem. C XXXX, XXX, XXX−XXX

be respected in the limit of highly diluted systems and that temperature is constant allows connecting L_{ii} to the corresponding diffusion coefficient D_i

$$D_i = \frac{k_B T L_{ii}}{\theta_i \theta_{*,i}} \tag{12}$$

(see, for example,[24] for more details).

Since the active sites for O and for VO_x species are expected to be different, we set $\theta_{*,O} = 1 - \theta_O$ and $\theta_{*,M} = \theta_{*,P} = 1 - \theta_M - \theta_P$. Extracting L_{ii} from eq 12, the diffusion flux for O reads

$$\mathbf{J}_O = -D_O \nabla \theta_O(\mathbf{r}) \tag{13}$$

while the diffusive flux for M is

$$\mathbf{J}_M = -D_M[(1 - \theta_P(\mathbf{r}))\nabla\theta_M(\mathbf{r}) + \theta_M(\mathbf{r})\nabla\theta_P(\mathbf{r})] \tag{14}$$

The reason why the latter flux is not of the Fick type is that the fraction of available empty sites depends not only on θ_M but also on θ_P. For P, we must take into account that the corresponding chemical potential reads

$$\mu_P(\mathbf{r}) = \mu_P^0 + k_B T \ln \theta_P(\mathbf{r}) + U(\mathbf{r})$$

so that a force related to the lateral interactions appears in the diffusion flux

$$\mathbf{J}_P = -D_P\left[(1 - \theta_M(\mathbf{r}))\nabla\theta_P(\mathbf{r}) + \theta_P(\mathbf{r})\nabla\theta_M(\mathbf{r}) + \theta_P(\mathbf{r})(1 - \theta_P(\mathbf{r}) - \theta_M(\mathbf{r}))\frac{\nabla U(\mathbf{r})}{k_B T}\right] \tag{15}$$

Reaction-Diffusion Equations. We hereby summarize the different contributions to the time evolution of the local coverages. For each species, the mass balance equation reads

$$\frac{\partial \theta_i}{\partial t} = \sum_k \nu_{ik} R_k - \nabla \cdot \mathbf{J}_i \tag{16}$$

where k represents a given reaction and ν_{ik} is the stoichiometric coefficient of species i in this reaction. We do not note the spatial dependency anymore for readability. Remembering that $k_d \ll k_r$, this gives for the species under consideration

$$\frac{\partial \theta_M}{\partial t} = k_D \theta_O \theta_P^2 \exp\left[\frac{2U}{k_B T}\right] - k_P(1 - \theta_O)\theta_M \theta_P \exp\left[\frac{U}{k_B T}\right] - \nabla \cdot \mathbf{J}_M \tag{17}$$

$$\frac{\partial \theta_P}{\partial t} = k_P(1 - \theta_O)\theta_M \theta_P \exp\left[\frac{U}{k_B T}\right] - k_D \theta_O \theta_P^2 \exp\left[\frac{2U}{k_B T}\right] - \nabla \cdot \mathbf{J}_P \tag{18}$$

$$\frac{\partial \theta_O}{\partial t} = k_P(1 - \theta_O)\theta_M \theta_P \exp\left[\frac{U}{k_B T}\right] - k_D \theta_O \theta_P^2 \exp\left[\frac{2U}{k_B T}\right] + 2k_a(1 - \theta_O)^2 - k_r^0 \theta_O \exp(\gamma \theta_P) - \nabla \cdot \mathbf{J}_O \tag{19}$$

where the fluxes are given by eqs 13−15. Our objective is to identify which qualitative type of dynamics these equations can generate under conditions that are similar to those of the experiments. The order of magnitude of some of the constants used can be obtained from experimental data (see Table 1). The other constants were treated as fitting parameters.

Table 1. Values Taken by the Constants in Our Simulations of eqs 17−19[a]

constant	description	value in simulations	experimental value
k_D	depolymerization	100 s^{-1}	
k_P	polymerization	1000 s^{-1}	
k_a	O_2 adsorption	(0.1/1) s^{-1}	13.6 s^{-1} (refs 28, 29)
k_r^0	unpromoted reaction	(0.01/0.1/0.7) s^{-1}	
γ	promotion by VO_x polymer	2/7	
u	interaction potential	−9/−7.5/−6.8	
σ	interaction length	0.2 μm	
D_M	diffusion of monomer	20 $\mu m^2\ s^{-1}$	[b] 18 $\mu m^2\ s^{-1}$ (ref 16)[b]
D_P	diffusion of polymer	0.1 $\mu m^2\ s^{-1}$	
D_O	diffusion of oxygen	50 $\mu m^2\ s^{-1}$	290 $\mu m^2\ s^{-1}$ (ref 30)[c]

[a]The experimental values at 750 °C and for a partial pressure of O_2 of 1×10^4 mbar are given for illustration, when available. [b]From $Rh(111)/V_6O_{12}$. [c]From Pt(111)/O.

Before showing and discussing the result of numerical integrations of eqs 17−19, we shortly discuss the limit of homogeneous systems.

PHASE TRANSITIONS IN HOMOGENEOUS SYSTEMS

The kinetic model defined by eqs 17−19 predicts the coexistence of several phases for a range of parameter values. This can already be seen by considering the homogeneous limit, for which

$$\nabla \cdot \mathbf{J}_i = 0 \tag{20}$$

and

$$U = u_0 \theta_P \tag{21}$$

The evolution equations now read

$$\frac{d\theta_M}{dt} = k_D \theta_O \theta_P^2\, e^{2u\theta_P} - k_P\,(1 - \theta_O)\theta_M \theta_P\, e^{u\theta_P} \tag{22}$$

$$\frac{d\theta_P}{dt} = k_P(1 - \theta_O)\theta_M \theta_P\, e^{u\theta_P} - k_D \theta_O \theta_P^2\, e^{2u\theta_P} \tag{23}$$

$$\frac{d\theta_O}{dt} = k_P(1 - \theta_O)\theta_M \theta_P\, e^{u\theta_P} - k_D \theta_O \theta_P^2\, e^{2u\theta_P} + 2k_a(1 - \theta_O)^2 - k_r^0 \theta_O\, e^{\gamma\theta_P} \tag{24}$$

where we have introduced $u = u_0/k_B T$.

Equations 22−24 can admit multiple steady states. Noting that $\theta_M + \theta_P = \theta$ is constant, we observe that the steady states (here denoted with overlines) are given by

$$k_D \bar{\theta}_O \bar{\theta}_P^2\, e^{2u\bar{\theta}_P} - k_P(1 - \bar{\theta}_O)(\theta - \bar{\theta}_P)\,\bar{\theta}_P\, e^{u\bar{\theta}_P} = 0 \tag{25}$$

$$2k_a(1 - \bar{\theta}_O)^2 - k_r^0 \bar{\theta}_O\, e^{\gamma\bar{\theta}_P} = 0 \tag{26}$$

Solving eq 26 for $\bar{\theta}_O$ yields a single physically acceptable solution (i.e., a coverage comprised between 0 and 1)

DOI: 10.1021/acs.jpcc.9b00427
J. Phys. Chem. C XXXX, XXX, XXX−XXX

$$\bar{\theta}_O = 1 + \frac{K e^{\gamma\bar{\theta}_P}}{4} - \frac{1}{4}\sqrt{8K e^{\gamma\bar{\theta}_P} + K^2 e^{2\gamma\bar{\theta}_P}} \quad (27)$$

with $K = k_r^0/k_a$. The resulting general solution for $(\bar{\theta}_P, \bar{\theta}_O)$ is rather intricate but can be simplified by noting that we consider systems for which $K\exp(\gamma\bar{\theta}_P)$ is expected to be large. Equation 27 can then be expanded in powers of $K^{-1}\exp(-\gamma\bar{\theta}_P)$, which leads to the dominant order to

$$\bar{\theta}_O \approx 2\frac{e^{-\gamma\bar{\theta}_P}}{K} \quad (28)$$

The steady-state coverage in P is thus given in this limit by substituting eqs 28 in 25

$$\frac{2\bar{\theta}_P e^{(u-\gamma)\bar{\theta}_P}}{KK_P} - (\theta - \bar{\theta}_P)\left(1 - 2\frac{e^{-\gamma\bar{\theta}_P}}{K}\right) = 0 \quad (29)$$

where $K_P = k_P/k_D$ is the polymerization equilibrium constant and where we excluded the special case $\bar{\theta}_P = 0$.

The coordinates for the critical point signaling the transition from a single stable steady state to multistationarity can be obtained by looking for conditions under which eq 29 switches from admitting a single to admitting multiple solutions. Solving this equation for K_P to the leading order in $K^{-1}\exp(-\gamma\bar{\theta}_P)$, we conclude that such a transition occurs at a critical point whose coordinates are

$$\bar{\theta}_P^{(c)} = \frac{\theta}{2};\ K_P^{(c)} = \frac{2e^{-2}}{K};\ (\gamma - u)^{(c)} = \frac{4}{\theta} \quad (30)$$

where the (c) superscript stands for "criticality". In terms of controllable parameters, criticality can be crossed either by changing the total amount of initial VO_x in the system (that is, by varying θ), by controlling temperature (which affects the equilibrium constants as well as u and γ), or by varying the pressure of O_2 or of X (since K depends on both k_r^0 and k_a). Beyond the critical point, the system admits three steady states. Standard linear analysis shows that the states with the higher and the lower polymer coverages are stable, while the intermediate state is unstable. These are characteristic properties of gas−liquid-like phase transitions, which are often found in lattice systems with interactions.[31] In our framework, the polymerized vanadium oxide would play the role of a two-dimensional liquid phase, while the monomers would be representative of a two-dimensional gas phase.

In the experiments on the VO_x/Rh(111) system, temperature and oxygen pressure are usually maintained constant and the reactivity is tuned by varying the pressure of reactant X. These experiments revealed that an initially featureless surface would present two distinct phases upon increasing this pressure: a vanadium-rich phase on one hand and a vanadium-poor phase on the other hand. In our model, a similar procedure would consist in maintaining all parameters constant except for K, which is itself proportional to the reaction rate constant. Figure 3 plots the stationary values $\bar{\theta}_P$ as a function of K, obtained by solving eqs 25−26. At low K, the system is found in a single state corresponding to a low density of polymers (high concentration of monomers). Above a given critical K value, two states can coexist, which correspond to the previous monomer-rich state and to a polymer-rich phase, as observed in experiments. For even larger K, most of the vanadium is predicted to be in the polymerized state. The fact that our model predicts phase coexistence in qualitative accordance with experiments is a sign that it retains the most important features of the system we are modeling here.

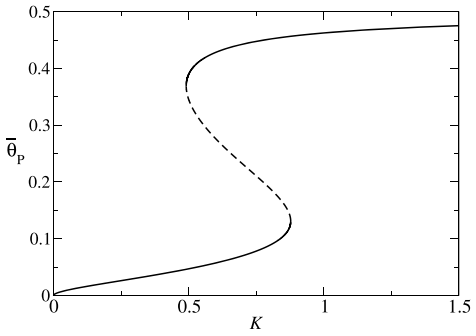

Figure 3. Steady-state solutions for the coverage in polymer, $\bar{\theta}_P$, obtained by solving eqs 25−26 with $K_P = k_P/k_D = 0.1$, $\theta = 0.5$, $u = -9$, and $\gamma = 2$.

SPATIOTEMPORAL SIMULATIONS

In this section, we show and analyze the result of numerical integrations of the full evolution equations, eqs 17−19. We used a forward-time, centered-space finite difference scheme with a spatial step $dr = 5.0 \times 10^{-2}$ μm and a time step $dt = 1.0 \times 10^{-4}$ s. One of our main objectives is to verify whether the proposed model has the same qualitative features as the experiments it is inspired from. We thus focus on parameter values that are in qualitative accordance with the experimental situation. In particular, the diffusion coefficients are always taken such that $D_O > D_M \gg D_P$. To mimic experimental conditions, we also always start from a surface that is almost exclusively covered with monomers.

Phase Separation and Cluster Formation. Numerical simulations show that for parametric conditions corresponding to monostability, the coverages of the various species remain homogeneous in space. This means that although the model is characterized by non-Fickian diffusion fluxes (due to site exclusion and to the presence of an interaction potential), the steady states are stable with respect to inhomogeneous perturbations and spatial instabilities, such as Turing instabilities, do not develop.

The situation changes when entering the zone of bistability. Starting from a given total coverage θ that is homogeneously distributed in space, the system spontaneously reorganizes into spatially distinct regions corresponding to either a P-rich phase or a P-depleted one. An example of such reorganization is given in Figure 4 in the case of a one-dimensional system and in Figure 5 for a two-dimensional system. Figure 6 plots the coverages of the different species obtained from a radial cut of a P-rich region. We observe that these zones are not only rich in polymer but also poor in both M and O. The concentration of P is maximal in the center of the island (with coordinate $r = 0$ in the graph) and rapidly decreases only after a given distance from the center has been attained, thereby forming well-defined islands with sharp boundaries.

The transition from the homogeneous to the spatially clustered states bears the typical signature of spinodal decomposition. For short times, we observe a rather rapid nucleation and growth of P-rich islands. The system then enters a slower regime during which evaporation of small "droplets" and coalescence of domains both take place. These two mechanisms induce a coarsening dynamics, which leads, for long times, to systems characterized by the coexistence of

DOI: 10.1021/acs.jpcc.9b00427
J. Phys. Chem. C XXXX, XXX, XXX−XXX

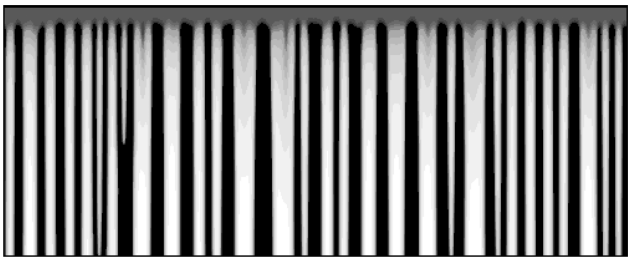

Figure 4. Spatiotemporal map of the concentration in P, θ_P, with dark regions corresponding to large values. Space (horizontal) spans over 500 μm, and time (vertical) goes from 0 s (top) to 100 s (bottom). The constants are as follows: $k_P = 100\ s^{-1}$, $k_D = 1000\ s^{-1}$ ($K_P = 0.1$); $k_r^0 = 0.7\ s^{-1}$, $k_a = 1.0\ s^{-1}$ ($K = 0.7$). The diffusion coefficients are $D_M = 20\ \mu m^2\ s^{-1}$, $D_P = 0.1\ \mu m^2\ s^{-1}$, and $D_O = 500\ \mu m^2\ s^{-1}$ and the characteristic distance σ is 0.2 μm. The other parameters are the same as in Figure 3. The initial conditions are $\theta_P = 0.05$, $\theta_M = 0.45$ (plus small fluctuations), and $\theta_O = 0$.

two separate homogeneous phases corresponding to the steady states reported in the analysis of the homogeneous system. The structures appearing in Figures 4 and 5 are thus only temporary, contrary to stationary dissipative structures that have been reported before for similar surface reactions.[22] In the latter case, the inhomogeneity is the result of a Turing instability, while in the present case, clusters appear and grow in relation to a phase transition. Consequently, the "wavelength" of the patterns appearing in our model is not constant but continuously increases in time until the final phase coexistence regime is attained. A similar coarsening has been observed in the VO_x/Rh(111) experiments: for example, in the $H_2 + O_2$ system, the length scale of the striped patterns was observed to increase as $\lambda \propto t^{\alpha}$ with α ranging between 0.23 and 0.25.[10]

These results all point to the idea that experimental observations of VO_x stripes and islands, just like the spatially extended version of the present model, correspond to spinodal decomposition. We still need to understand however why movement of macroscopic islands is observed only under reactive conditions. We treat this specific question in the next subsection.

Island Movement and Merging. Experiments revealed that upon increase of the reaction rate between oxygen and reactant X, the shape and size of the islands change. Under certain conditions, these morphological changes can also be accompanied by a new type of coarsening mechanism, in which mesoscopic islands start to move toward each other until they merge.

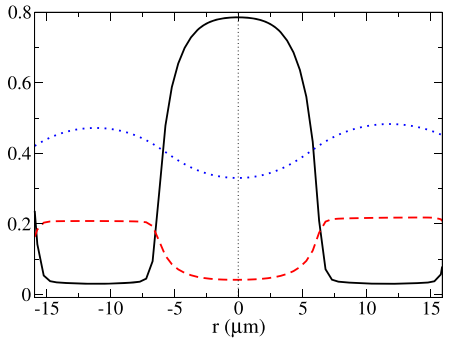

Figure 6. Coverages in P (black full line), M (red dashed line), and O (blue dotted line) across a P-rich region. These curves were obtained from the spatial distribution at $t = 100$ s in Figure 4.

Interestingly, similar features are observed in the simple model that we developed here. For appropriate values of the parameters, increasing the reaction rate by increasing either k_a, k_r^0, or both these parameters leads, for short times, to the evaporation of small islands and to a small increase in size of the already larger islands. This change is characteristic of the classical Ostwald ripening.[32] For longer times, however, we observe that some of the islands start to move toward each other and merge. This can be seen in Figure 7 for a one-dimensional system. These island movements are similar to Smoluchowski ripening. However, they only take place under reactive conditions, for reasons that we explain below.

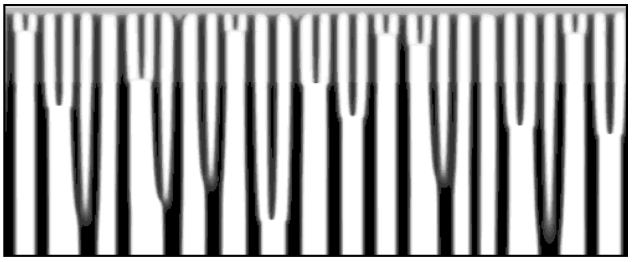

Figure 7. Spatiotemporal map showing the evolution of the density of P species upon increasing the reactivity. The total time is 1000 s, and the size of the system is 500 μm. The parameters are the same as in Figures 4 and 6, except for u (=−7.5), γ (=7), and for k_a and k_r^0. For short times (low reactivity), $k_a = 0.1\ s^{-1}$ and $k_r^0 = 0.01\ s^{-1}$, while starting at $t = 300$ s, the system is put into more reactive conditions ($k_a = 1\ s^{-1}$ and $k_r^0 = 0.1\ s^{-1}$). The initial condition is $\theta_P = 0.05$, $\theta_M = 0.4$ (with small fluctuations), and $\theta_O = 0$.

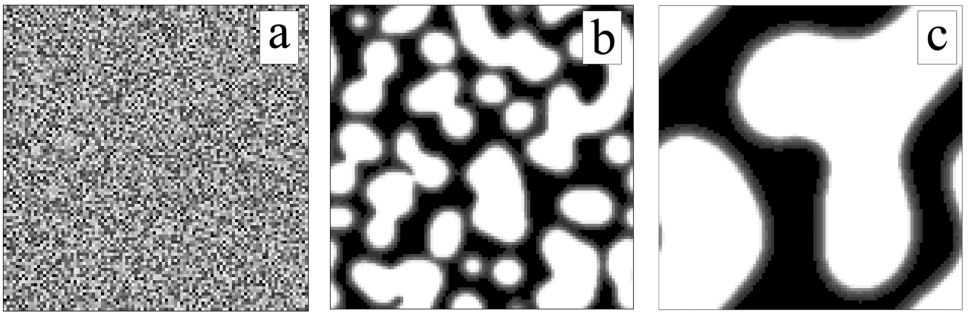

Figure 5. Snapshots of the concentration in P in a (100 × 100) μm^2 two-dimensional system for (a) $t = 0$ s, (b) $t = 100$ s, and (c) $t = 500$ s. Parameters and initial conditions are the same as in Figure 4.

DOI: 10.1021/acs.jpcc.9b00427
J. Phys. Chem. C XXXX, XXX, XXX−XXX

As depicted in Figure 8, the distance between the island centers is constant for short times but then starts decreasing in

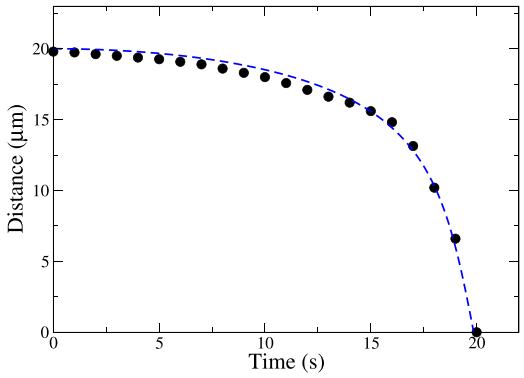

Figure 8. Distance between two island centers, with parameters identical to those in Figure 7. Time zero corresponds here to the time where the reactive conditions are turned on. The blue dashed curve was obtained from a numerical integration of eq 34, with $\sigma_I = 0.6\ \mu$m and $u_0\theta_P^0/\sqrt{2\pi}\sigma_I^3\Omega = -1 \times 10^{-3}$.

an accelerating fashion until merging occurs. Very similar curves were obtained in the experiments.[13]

Simulations in two dimensions give similar results (see Figure 9). Some of the initial islands evaporate (compare

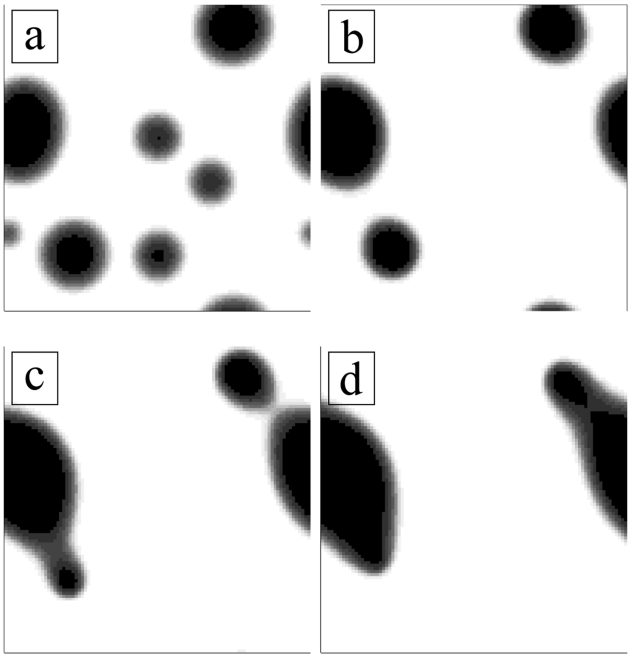

Figure 9. Simulations in two dimensions. The linear size of the system is 50 μm. The parameters are the same as in Figure 7, except for $u = -6.8$ and an initial monomer coverage $\theta_M = 0.3$. The four snapshots are taken at times $t = 0$ s (a), 30 s (b), 80 s (c), and 130 s (d) ($t = 0$ corresponds to the time when the reactive conditions are turned on).

Figure 9a,b), while the largest ones slightly grow and then start moving toward each other. Note that as they move, the islands tend to deform (they become droplike) but that they become round again after merging. The main difference with one-dimensional simulation results is that the region of parameters where island movement and merging can be observed is more limited.

As mentioned earlier, it was proposed that the propagation is mainly due to a polymerization/depolymerization equilibrium between islands that is controlled by the oxygen coverage.[13] The main idea is that the oxygen coverage between two remote islands reaches high values, which favors depolymerization. In terms of the model hereby developed, this would translate into a high value of θ_M and θ_O between these islands. If on the other hand two islands are separated by short distances, the oxygen coverage in the inter-island space remains low, which favors polymerization and thus the islands "grow" toward each other. Our simulations show that the islands that we observe moving toward each other are those that were sufficiently close so that the oxygen coverage is low enough and the rate of polymer formation is high (see Figure 7, for example). The merging of islands is accompanied by a drastic change in the gradient of oxygen. There is initially a maximum of oxygen coverage between the islands. As they move toward each other and merge, the concentration of oxygen first increases and then rapidly decreases so that its coverage presents a minimum inside the newly formed island (see Figure 10).

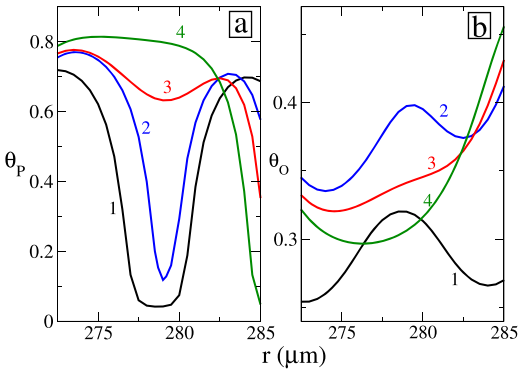

Figure 10. Coverages in P (a) and O (b) during the merging of two nearby islands. The conditions are the same as in Figure 7. Time is respectively $t = 600$ s (black curve with label 1), 700 s (blue curve with label 2), 800 s (red curve with label 3), and 900 s (green curve with label 4).

It should be emphasized that γ and D_O play an important role in the merging of islands. Island movement is observed only when γ and D_O are large enough. This can be understood qualitatively by the fact that large values of these parameters tend to increase both the island size and the distance over which the oxygen gradients extend around islands. Large values of γ make depletion of oxygen inside the P-rich islands important enough so that the inter-island space is poor in adsorbed O, and large values of D_O ensure that this O-poor region extends over large distances. These combined effects define a sort of "critical radius of interaction" around each island, below which two neighboring islands start interacting strongly enough so that they can start moving toward each other. When γ and D_O are small, this radius is very small and merging is thus very rare.

In conclusion, our theoretical model fully supports the previously proposed mechanism.[13] The results of simulations moreover allow us to study in more detail the different stages of this new ripening mechanism. The merging of islands can in fact be seen, in the framework of the present model, as a four-stage process. First, increasing the reactivity leads to a small increase in size of some islands. This increase allows for the appearance of islands separated by distances that are relatively

DOI: 10.1021/acs.jpcc.9b00427
J. Phys. Chem. C XXXX, XXX, XXX−XXX

short. In a second time, the boundaries of two close-enough islands start to grow toward each other because they are surrounded by a monomer-rich medium where the oxygen-poor conditions are now such that polymerization occurs. In a third phase, the deformation of the island due to the displaced boundaries leads to a movement of this island as a whole. The latter phenomenon is due to the fact that P species present strong interactions. When an island deforms in one direction, the individual P units forming the rest of the island slowly diffuse toward the burgeoning part since they are attracted by other P species. Finally, the boundaries of the two islands involved in the process become close enough so that they attract each other and the remaining M species can polymerize and fill the gap between them.

Equation of Motion for the Islands. Thanks to the simplicity of the model proposed here, the shape of the position vs time plots in the third and fourth phases of the ripening process can be qualitatively reproduced on the basis of mechanical arguments. Consider in a one-dimensional system an island centered on a position r_0, separated from another island whose center is located at a distance L. Assuming Gaussian-shaped islands, the potential felt at the point of reference r_0 is given by

$$U = \int_0^\infty u(r) \frac{\theta_P^0}{\sqrt{2\pi\sigma_I^2}} \exp\left[-\frac{(r-L)^2}{2\,\sigma_I^2}\right] dr \tag{31}$$

where θ_P^0 is the maximal polymer concentration in the island and σ_I is a measure of its width. Note that r is here the position relative to r_0. Using eq 8 for the interaction potential $u(r)$ yields

$$U = \frac{u_0\theta_P^0}{\sqrt{2(\sigma^2+\sigma_I^2)}} \exp\left(-\frac{L^2}{2(\sigma^2+\sigma_I^2)}\right) \approx \frac{u_0\theta_P^0}{\sqrt{2\pi}\,\sigma_I} \exp\left(-\frac{L^2}{2\,\sigma_I^2}\right) \tag{32}$$

since we are considering mesoscopic islands and short-ranged interactions ($\sigma \ll \sigma_I$). Consequently, the force exerted by an island located at distance L is given by

$$F = -\nabla U = \frac{u_0\theta_P^0}{\sqrt{2\pi}\,\sigma_I^3} L \exp\left(-\frac{L^2}{2\sigma_I^2}\right) \tag{33}$$

Note that F depends non-monotonously on L: the force is low for short and long distances and goes through an extremum located at $L^* = \sigma_I$. Distances $L < L^*$ correspond to situations where the impenetrability of islands, which we did not include in our reasoning, starts playing a role. We should thus expect our approximate expression for the force to be valid only for distances that are larger than σ_I, which means that in its range of validity, the force decreases monotonously (in absolute value) from $L = \sigma_I$ to $L = \infty$.

Our basic hypothesis now is that the equation for the inter-island distance is given by an effective Newton law

$$\Omega \frac{d^2L}{dt^2} = F = \frac{u_0\theta_P^0}{\sqrt{2\pi}\,\sigma_I^3} L \exp\left(-\frac{L^2}{2\,\sigma_I^2}\right) \tag{34}$$

where Ω plays the role of an effective mass. Numerical integration of eq 34 yields trajectories whose shapes are very similar to those obtained with simulations of the full model, eqs 17−19. This can be seen for example in Figure 8, where the dashed curve represents the result of such an integration. This suggests that the motion of islands is mainly dictated by the force related to interactions that they exert upon each other.

CONCLUSIONS

In this work, we proposed and analyzed a simple reaction model aimed at reproducing (qualitatively) the new ripening mechanism recently observed experimentally during reaction-induced redistribution of vanadium oxide (VO_x) films on rhodium.[13] The model predicts that the formation of VO_x-rich polymerized islands observed in experiments corresponds to a combination of phase transition and chemical reaction, with the source of the phase transition residing in the strong interactions between polymerized VO_x entities inside the islands. The movement and merging of islands observed under reactive, nonequilibrium conditions can be interpreted as being due to a combination of a "chemical force" (the polymerization process) and a "physical force" (the force due to lateral interactions): the polymerization process between islands allows them to start interacting via physical interactions, which deforms them and consequently triggers a movement of the islands because of the cohesion provided by the strongly attractive interactions between polymerized units.

In a sense, one could say that the mechanism at play is similar to Smoluchowski ripening because it involves the movement and subsequent collision of large islands. Contrary to this classical mechanism, however, the movement of islands is here due to a chemical reaction that induces a directed motion only in the presence of sufficiently strong chemical gradients. It is thus rather a form of chemotactic ripening. The model that we studied here was designed so as to be as generic as possible. This suggests that other systems having similar features could display the same unconventional ripening mechanism.

AUTHOR INFORMATION

Corresponding Author

*E-mail: ydedecke@ulb.ac.be.

ORCID

Yannick De Decker: 0000-0002-7493-9657

Ronald Imbihl: 0000-0002-5155-7250

Notes

The authors declare no competing financial interest.

ACKNOWLEDGMENTS

The authors would like to thank B. von Boehn for providing details and for fruitful discussions concerning experiments and A. S. Mikhailov for useful comments and stimulating discussions.

REFERENCES

(1) Slinko, M. M.; Jaeger, N. I. Oscillating Heterogeneous Catalytic Systems. In *Studies in Surface Science and Catalysis*; Delmon, B., Bates, J. T., Eds.; Elsevier: Amsterdam, 1994; Vol. *86*.

(2) Imbihl, R.; Ertl, G. Oscillatory Kinetics in Heterogeneous Catalysis. *Chem. Rev.* **1995**, *95*, 697−733.

(3) Imbihl, R. Nonlinear Dynamics on Catalytic Surfaces: The Contribution of Surface Science. *Surf. Sci.* **2009**, *603*, 1671−1679.

(4) Nicolis, G.; Prigogine, I. *Self-Organization in Nonequilibrium Systems: From Dissipative Structures to Order through Fluctuations*; Wiley-Blackwell, 1977.

DOI: 10.1021/acs.jpcc.9b00427
J. Phys. Chem. C XXXX, XXX, XXX−XXX

(5) Schoiswohl, J.; Surnev, S.; Sock, M.; Ramsey, M. G.; Kresse, G.; Netzer, F. P. Thermodynamically Controlled Self-Assembly of Two-Dimensional Oxide Nanostructures. *Angew. Chem., Int. Ed.* **2004**, *43*, 5546−5549.
(6) Schoiswohl, J.; Sock, M.; Eck, S.; Surnev, S.; Ramsey, M. G.; Netzer, F. P.; Kresse, G. Atomic-level Growth Study of Vanadium Oxide Nanostructures on Rh(111). *Phys. Rev. B* **2004**, *69*, No. 155403.
(7) Schoiswohl, J.; Surnev, S.; Netzer, F. P. Reactions on Inverse Model Catalyst Surfaces: Atomic Views by STM. *Top. Catal.* **2005**, *36*, 91−105.
(8) Schoiswohl, J.; Surnev, S.; Netzer, F. P.; Kresse, G. Vanadium Oxide Nanostructures: From Zero- to Three-dimensional. *J. Phys.: Condens. Matter* **2006**, *18*, R1−R14.
(9) Schoiswohl, J.; Sock, M.; Chen, Q.; Thornton, G.; Kresse, G.; Ramsey, M. G.; Surnev, S.; Netzer, F. P. Metal Supported Oxide Nanostructures: Model Systems for Advanced Catalysis. *Top. Catal.* **2007**, *46*, 137−149.
(10) Lovis, F.; Imbihl, R. Self-organization of Ultrathin Vanadium Oxide Layers on a Rh(111) Surface during a Catalytic Reaction. Part I: A PEEM Study. *J. Phys. Chem. C* **2011**, *115*, 19141−19148.
(11) Lovis, F.; Hesse, M.; Locatelli, A.; Menteş, T. O.; Niño, M. A.; Lilienkamp, G.; Borkenhagen, B.; Imbihl, R. Self-organization of Ultrathin Vanadium Oxide Layers on a Rh(111) Surface during a Catalytic Reaction. Part II: A LEEM and Spectromicroscopy Study. *J. Phys. Chem. C* **2011**, *115*, 19149−19157.
(12) Imbihl, R. Chemical Selforganization of Composite Catalysts during Catalytic Reactions. *J. Electron Spectrosc. Relat. Phenom.* **2012**, *185*, 347−355.
(13) Hesse, M.; Von Boehn, B.; Locatelli, A.; Sala, A.; Menteş, T. O.; Imbihl, R. Island Ripening via a Polymerization-Depolymerization Mechanism. *Phys. Rev. Lett.* **2015**, *115*, No. 13610.
(14) Von Boehn, B.; Preiss, A.; Imbihl, R. Dynamics of Ultrathin V-oxide Layers on Rh(111) in Catalytic Oxidation of Ammonia and CO. *Phys. Chem. Chem. Phys.* **2016**, *18*, 19713−19721.
(15) Von Boehn, B.; Mehrwald, S.; Imbihl, R. Hole Patterns in Ultrathin Vanadium Oxide Layers on a Rh(111) Surface during Catalytic Oxidation Reactions with NO. *Chaos* **2018**, *28*, No. 045117.
(16) Schoiswohl, J.; Kresse, G.; Surnev, S.; Sock, M.; Ramsey, M. G.; Netzer, F. P. Planar Vanadium Oxide Clusters: Two-Dimensional Evaporation and Diffusion on Rh(111). *Phys. Rev. Lett.* **2004**, *92*, No. 206103.
(17) Romanyshyn, Y.; Guimond, S.; Kuhlenbeck, H.; Kaya, S.; Blum, R. P.; Niehus, H.; Shaikhutdinov, S.; Simic-Milosevic, V.; Nilius, N.; Freund, H.-J.; Ganduglia-Pirovano, M. V.; Fortrie, R.; Döbler, J.; Sauer, J. Selectivity in Methanol Oxidation as Studied on Model Systems Involving Vanadium Oxides. *Top. Catal.* **2008**, *50*, 106−115.
(18) Einstein, T. L.; Schrieffer, J. R. Indirect Interaction between Adatoms on a Tight-Binding Solid. *Phys. Rev. B* **1973**, *7*, 3629−3648.
(19) Verdasca, J.; Borckmans, P.; Dewel, G. Chemically Frozen Phase Separation in an Adsorbed Layer. *Phys. Rev. E* **1995**, *52*, No. R4616.
(20) Hildebrand, M.; Mikhailov, A. S.; Ertl, G. Nonequilibrium Stationary Microstructures in Surface Chemical Reactions. *Phys. Rev. E* **1998**, *58*, No. 5483.
(21) Hildebrand, M.; Mikhailov, A. S.; Ertl, G. Traveling Nanoscale Structures in Reactive Adsorbates with Attractive Lateral Interactions. *Phys. Rev. Lett.* **1998**, *81*, No. 2602.
(22) De Decker, Y.; Marbach, H.; Hinz, M.; Günther, S.; Kiskinova, M.; Mikhailov, A. S.; Imbihl, R. Promoter-Induced Reactive Phase Separation in Surface Reactions. *Phys. Rev. Lett.* **2004**, *92*, No. 198305.
(23) De Decker, Y.; Mikhailov, A. S. Promoter-Induced Nonlinear Pattern Formation in Surface Chemical Reactions. *J. Phys. Chem. B* **2004**, *108*, 14759−14765.
(24) De Decker, Y.; Mikhailov, A. S. Nanoscale Pattern Formation inNon-Equilibrium Surface Chemical Reactions. *Prog. Theor. Phys. Suppl.* **2006**, *165*, 119−143.
(25) Prigogine, I.; Defay, R. *Chemical Thermodynamics*; Wiley, 1954.
(26) Prigogine, I. *Etude Thermodynamique des Processus Irréversibles*; Desoer, 1947.
(27) de Groot, S. R.; Mazur, P. *Non-equilibrium Thermodynamics*; Dover Publications, 2011.
(28) Thiel, P. A.; Yates, J. T., Jr.; Weinberg, W. H. The Interaction of Oxygen with the Rh(111) Surface. *Surf. Sci.* **1979**, *82*, 22−44.
(29) Peterlinz, K. A.; Sibener, S. J. Absorption, Adsorption, and Desorption Studies of the Oxygen/Rh(111) System Using O_2, NO, and NO_2. *J. Phys. Chem.* **1995**, *99*, 2817−2825.
(30) Barth, J. V. Transport of adsorbates at metal surfaces: from thermal migration to hot precursors. *Surf. Sci. Rep.* **2000**, *40*, 75−149.
(31) Hildebrand, M.; Mikhailov, A. S. Mesoscopic Modeling in the Kinetic Theory of Adsorbates. *J. Phys. Chem.* **1996**, *100*, 19089−19101.
(32) Voorhees, P. W. Ostwald Ripening of Two-Phase Mixtures. *Annu. Rev. Mater. Sci.* **1992**, *22*, 197−215.

DOI: 10.1021/acs.jpcc.9b00427
J. Phys. Chem. C XXXX, XXX, XXX−XXX